





## Chapter 4

# The physics behind self-propagating layers

*Flows developing in initially doubly stratified systems are considered, i.e. in addition to a stabilizing salinity distribution a destabilizing temperature distribution is present. Lateral heating of such a system results in the formation of intrusions consisting of laterally expanding convection cells separated by diffusive interfaces. Although the development of the intrusions is qualitatively similar to that in singly stratified liquids, important differences occur when the initial destabilizing temperature gradient becomes large. When the lateral heating is turned off, intrusions are still able to propagate. The main contribution of the chapter is a detailed study of the physics of this self-propagation process.*

### 4.1 Introduction

Double-diffusive convection, i.e. convection in a stably stratified liquid due to different diffusivities of two components [Turner, 1973] is a potentially important mixing process of heat and salt in the ocean [Schmitt, 1994]. Clear signatures of this process are well mixed layers, separated by very stable interfaces over which only diffusive transport is possible. A typical case where these layers occur is a laterally heated liquid which is initially stably stratified through a constant vertical salt gradient. Laboratory experiments [Wirtz *et al.*, 1972; Jeevaraj and Imberger, 1991] have provided the scales of these layers in terms of parameters of the flow. In Chapter 3 of this thesis [Kranenborg and Dijkstra, 1996], which was concerned with the layer merging process of intrusions developing in an initially singly stratified liquid, the experimental results were shortly

---

#### 4. The physics behind self-propagating layers

---

reviewed. If the lateral temperature gradient is  $\Delta T$  and the initial density gradient  $\phi_0$ , then the characteristic layer scale is

$$\eta = \frac{\alpha \Delta T}{\beta \phi_0} \quad (4.1)$$

where  $\alpha$  and  $\beta$  are the expansion coefficients in the linear equation of state relating density changes to temperature and salinity changes, respectively.

In experiments, also situations have been considered in which, apart from a stabilizing salt gradient  $\frac{\partial S_0}{\partial z}$ , a destabilizing temperature gradient  $\frac{\partial T_0}{\partial z}$  was initially present [Jeevaraj and Imberger, 1991; Schladow *et al.*, 1992]. Motivation for these experiments was the potential ability to tap energy from the initial thermal stratification. Layers may continue to propagate even when sidewall forcing is turned off, a process called self-propagation. The doubly stratified systems are particularly interesting in an oceanographic context because the presence of an additional unstable temperature gradient is common in the upper parts of the ocean [Jacobs *et al.*, 1981].

Jeevaraj and Imberger [1991] anticipated the self-propagation of intrusions for relatively low values of the vertical stability ratio  $R_\rho$ , defined as

$$R_\rho = \frac{\beta \frac{\partial S_0}{\partial z}}{\alpha \frac{\partial T_0}{\partial z}} \quad (4.2)$$

However, even at the smallest value of  $R_\rho = 2.5$ , they did not observe it.

Extensive experimental and numerical work on the evolution of intrusions in doubly stratified systems was presented in Schladow *et al.* [1992]. Instead of a wall temperature rise as in Jeevaraj and Imberger [1991], they use a constant lateral heat flux forcing  $q$ . They classify the flows according to the values of  $R_\rho$  and a lateral stability parameter  $R_l$ , defined as

$$R_l = \frac{\frac{\alpha q}{k}}{\alpha \frac{\partial T_0}{\partial z} - \beta \frac{\partial S_0}{\partial z}} \quad (4.3)$$

where  $k$  is the thermal conductivity. In the case of high lateral and gravitational stability (small  $R_l$  and large  $R_\rho$ , class I) the system behaves like the singly stratified case. Within the layers, the temperature is stably stratified and the salt is well mixed. As the lateral heating becomes more important (class II) convection becomes more vigorous and the layer thickness increases. The salinity is generally well mixed or slightly unstable stratified within the layers and convection due to salt-fingering is possible. In the case of very low gravitational and lateral stability (class III), both heat and salt are well-mixed within the layers. Under conditions of small  $R_\rho$  and relatively large  $R_l$ , self-propagation of layers is observed.

In this chapter, the evolution of intrusions into a doubly stratified liquid is studied through direct numerical simulation in a two-dimensional set-up. At a low stability ratio, self-propagation

of intrusions is found and several characteristics of this process are obtained. Based on the analysis of the numerical results, two energy sources for the self-propagation are identified. First, local instabilities which develop ahead of the intrusions may transfer energy used for the propagation. This source is similar to that proposed in *Schladow et al.* [1992]. Another source of energy is shown to come from the global adjustment of the density field.

## 4.2 Formulation

The model is similar to that in Chapter 3 but shortly repeated for convenience. A two-dimensional rectangular container (length  $L$  and height  $H$ ) is filled with a Newtonian liquid with a kinematic viscosity  $\nu$  and stratified through heat and salt with a constant thermal diffusivity  $\kappa_T$  and solutal diffusivity  $\kappa_S$ . The governing equations are non-dimensionalized using scales  $H$ ,  $H^2/\kappa_T$ ,  $\kappa_T/H$ ,  $\Delta S$  and  $\Delta T$  for length, time, velocity, salinity and temperature, respectively. The equations describing the evolution of the flow are the two-dimensional Navier-Stokes equations and the conservation equations of heat and salt given in Chapter 3 in terms of the streamfunction  $\psi$  and the vorticity  $\omega$ .

Apart from the Prandtl number  $Pr = \frac{\nu}{\kappa_T}$ , the Lewis number  $Le = \frac{\kappa_T}{\kappa_S}$  and the aspect ratio  $A = \frac{L}{H}$ , the relevant parameters in these equations are the thermal Rayleigh number  $Ra_T$ , the buoyancy ratio  $R$ , the length scale  $\eta$  and the Rayleigh number  $Ra_\eta$  based on  $\eta$

$$Ra_T = \frac{g\alpha\Delta TH^3}{\nu\kappa_T}, \quad R = \frac{\beta\Delta S}{\alpha\Delta T}, \quad \eta = H/R; \quad Ra_\eta = Ra_T/R^3 \quad (4.4)$$

At all boundaries no-slip conditions for velocity are prescribed. At the left sidewall, the heating rise curve is prescribed as

$$T(x=0, z, t) = 1 - \exp\left(-\frac{t}{t_0}\right) \quad (4.5)$$

and the right sidewall is assumed to be isolated. This situation is similar to that in the experiments by *Jeevaraj and Imberger* [1991]. All walls are impermeable to salt; in dimensionless form the remaining boundary conditions are

$$x=0: \frac{\partial S}{\partial x} = 0; \quad x=1: \frac{\partial T}{\partial x} = 0, \quad \frac{\partial S}{\partial x} = 0; \quad (4.6)$$

$$z=0: \frac{\partial S}{\partial z} = 0, \quad \frac{\partial T}{\partial z} = 0; \quad z=1: \frac{\partial S}{\partial z} = 0, \quad \frac{\partial T}{\partial z} = 0 \quad (4.7)$$

<i>dimensionless quantities</i>	
$A$	$= 1$
$Le$	$= 101$
$Pr$	$= 7$
$R$	$= 5$
$Ra_\eta$	$= 5 * 10^4$
$Ra_T$	$= 6.25 * 10^6$
$t_0$	$= 1 * 10^{-3}$
<i>dimensional quantities</i>	
$H$	$= 0.2 (m)$
$L$	$= 0.2 (m)$
$\kappa_S$	$= 1 * 10^{-9} (m^2 s^{-1})$
$\kappa_T$	$= 1 * 10^{-7} (m^2 s^{-1})$
$\nu$	$= 7 * 10^{-7} (m^2 s^{-1})$

Table 4.1: Values of both dimensionless and dimensional model parameters.

### 4.3 Results

A 'reference' experiment is defined by the values of the parameters as given in Table 4.1. As in Chapter 3, the thermal diffusion time scale is  $4 * 10^5 [s]$  and all dimensionless times below are with respect to this time. The initial conditions are different from those in Chapter 3 in that there is, in addition to a stabilizing salt gradient, now also a destabilizing temperature gradient. The initial conditions introduce the stability ratio  $R_\rho$  and become

$$t = 0 : T_0(x, z) = -RR_\rho^{-1}z ; S_0(x, z) = 1 - z. \tag{4.8}$$

The limiting singly stratified case is obtained as  $R_\rho \rightarrow \infty$ .

A value of  $R_\rho = 1.5$  is potentially in the regime of self-propagation [Schladow *et al.*, 1992]. To be able to make comparisons with the singly stratified flows in Chapter 3, the buoyancy ratio  $R$  is chosen such that the initial density gradient based on (4.8) is the same as the initial density gradient in the standard case in Chapter 3 ( $R = 5$ ); this results in  $R = 15$ . Due to the initial vertical temperature gradient, the lengthscale  $\eta$  and therefore the Rayleigh number  $Ra_\eta$  vary linearly with  $z$ . The initial temperature distribution and  $Ra_\eta$  were prescribed such that at  $z = 1/2 : Ra_\eta = 5 * 10^4$ , which is the standard value in Chapter 3. Hence, for  $z < 0.5$  ( $z > 0.5$ ) the buoyancy forcing is weaker (stronger) than that at  $z = 0.5$ , because the lateral temperature

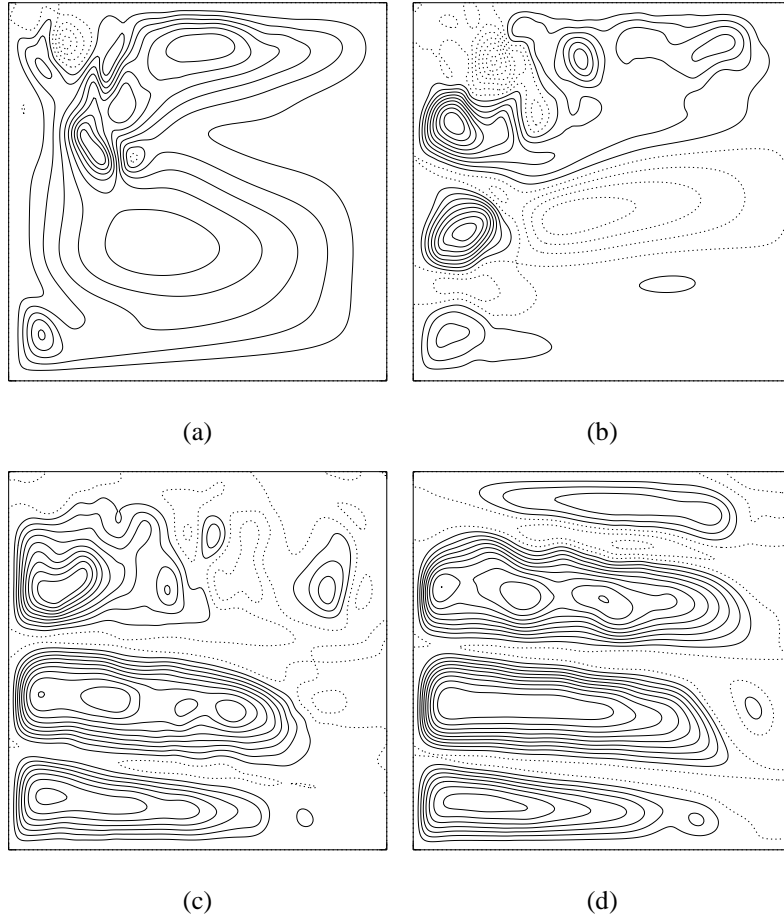


Figure 4.1: *Contour plots of the streamfunction, showing the development of layers in the doubly stratified case,  $Ra_\eta = 5 \cdot 10^4$ ,  $R = 5$ ; (a):  $t = 0.005$ , (b):  $t = 0.01$ , (c):  $t = 0.05$ , (d):  $t = 0.1$ .*

difference (between wall and liquid far from the heated wall) decreases with  $z$ .

#### 4.3.1 Flow characteristics

We first consider a cavity with aspect ratio  $A = 1$  as in Chapter 3 and use the same numerical methods and the same resolution ( $201 \times 201$  equidistant gridpoints). The layer development for the standard case  $Ra_\eta = 5 \cdot 10^4$  and  $R = 15$  is presented in the Figs. 4.1, where four snapshots of

#### 4. The physics behind self-propagating layers

---

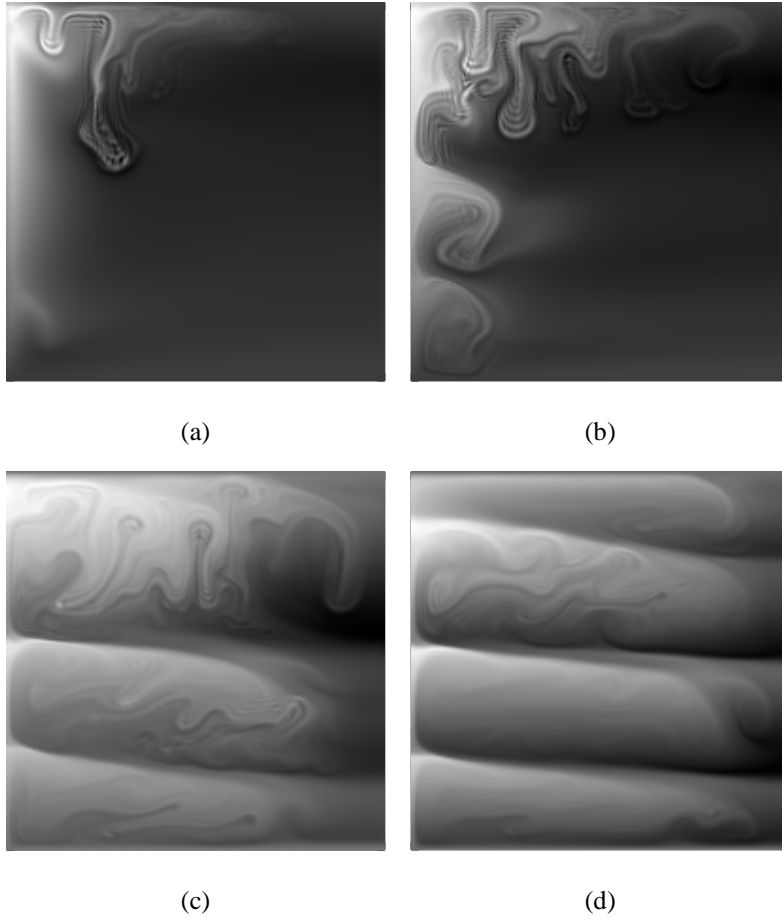


Figure 4.2: *Development of layers in the doubly stratified case for  $Ra_\eta = 5 \cdot 10^4$ ,  $R = 5$ . Shown is the salinity distribution minus the initial salinity distribution: white corresponds to relatively salty liquid, black corresponds with relatively fresh liquid. (a):  $t = 0.005$ , (b):  $t = 0.01$ , (c):  $t = 0.05$ , (d):  $t = 0.1$ .*

the flow field are shown as contour plots of the streamfunction. More details of the flow can be observed in the Figs. 4.2, where the difference of the actual salinity field and the initial salinity distribution are presented as a grey-shade plot. The latter salinity fields are also shown in the Figs. 4.3 at corresponding times for the singly stratified case with  $R_\rho = \infty$ ,  $R = 5$ .

In both singly and doubly stratified cases, layers develop within about 10 hours. However,

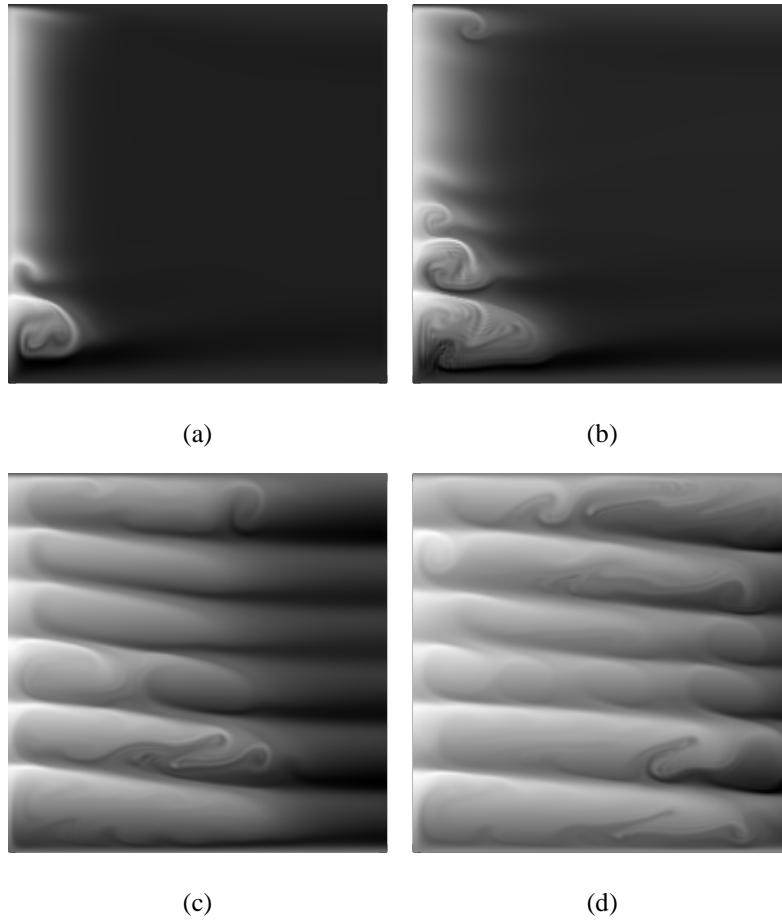


Figure 4.3: As Figure 4.2, but now for the singly stratified case at the same instants.

the initial development and the final scales of the layers are strikingly different for both cases. Whereas in the singly stratified case about 6 layers develop (Fig. 4.3c-d), the number of layers is smaller in the doubly stratified case. About 4 layers are observed (Fig. 4.2c-d), of which only the lower three are well-developed. For these three layers, the thickness increases upwards contrary to the layers in Fig. 4.3c-d whose thickness decreases upwards. The layer size is larger than that of the corresponding singly stratified flow, which is in accordance with the observations of *Jeevaraj and Imberger [1991]*.

Plots of the horizontal velocity, temperature, salinity and density along a section through the

#### 4. The physics behind self-propagating layers

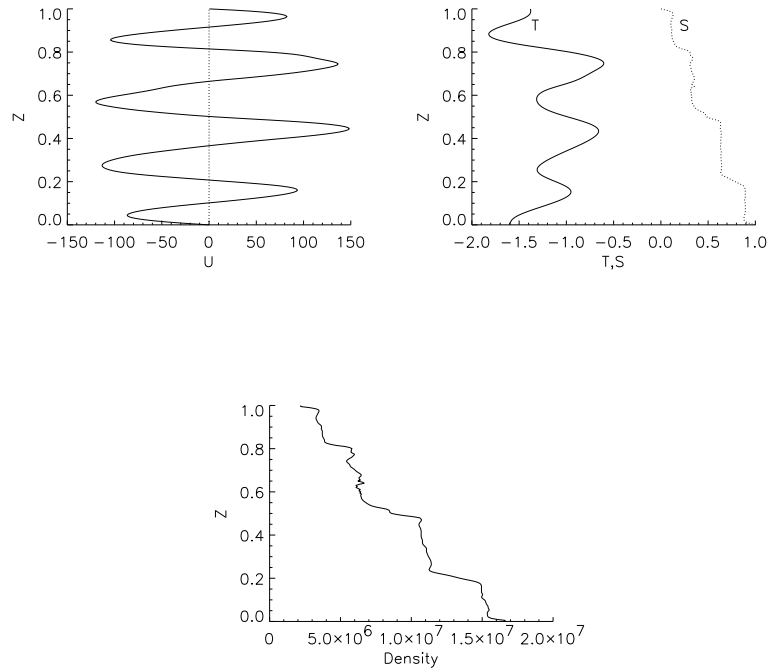


Figure 4.4: Horizontal velocity  $U$ , temperature  $T$ , salinity  $S$  and density  $\rho$  for the doubly stratified case at  $t = 0.1$  along a section through the middle of the container.

middle of the container ( $x = 0.5$ ) are shown at  $t = 0.1$  for the doubly stratified case in the Figs. 4.4. The horizontal velocities have a slightly smaller amplitude in the lower layer and nearly equal magnitude in the next two layers (Fig. 4.4a). Within each layer, the temperature is stably stratified whereas the salinity is well mixed (Fig. 4.4b). Over the interfaces separating the layers, the temperature is unstably stratified, similar to the distributions found in the singly stratified case (Chapter 3). The salinity profile in Fig. 4.4b also reveals the increase of layer thickness with height. The latter effect can easily be explained, since the layer thickness depends on the lateral temperature difference which varies with liquid height in the doubly stratified case. The density distribution is generally stable both in the layers and the interfaces between them (Fig. 4.4c).

A main difference between the flows in the Figs. 4.2 and the Figs. 4.3 is the convective activity in the upper layer which is much stronger for the doubly stratified case (compare Fig. 4.2a-b with Fig. 4.3a-b). Clear signatures of this strong convection are also shown in Fig. 4.1b-c. These features were also noted by *Schladow et al.* [1992] in their doubly stratified experiments. For instance, their Fig. 5a shows the same plume-like structures as those in the Figs. 4.2. This strong convection is absent in the singly stratified case (Figs. 4.3). The existence of flow with significant convective activity suggests that the simulated flow would fit into either class II or III of *Schladow et al.* [1992], but since the temperature is stably stratified within the layers (Fig. 4.4b), class II seems appropriate.

Although we prescribe no constant heat flux at the left wall, as in *Schladow et al.* [1992], we consider the magnitude of the lateral stability parameter  $R_l$  by computing the range of the heat flux in the simulation. The parameter  $R_l$ , as given in (4.3), can be expressed into our model parameters by nondimensionalization and using the values of the vertically averaged horizontal heat flux  $\overline{Nu}(x, t)$  (defined in Chapter 3) at the heated sidewall ( $x = 0$ ). This gives

$$R_l = \frac{\mathcal{H}_d \overline{Nu}(0, t)}{R(1 - R_\rho^{-1})} \quad (4.9)$$

where  $\mathcal{H}_d$  is the diffusive heat flux in absence of any flow (see Chapter 3). In the simulation above, with a constant temperature at the left sidewall, the heat transport varies significantly along the heated wall because  $Ra_\eta$  varies vertically. However, the value of  $R_l$  based on the averaged heat flux is in the range [4, 40]. For a typical case, with  $\mathcal{H}_d \overline{Nu} = 60$  ( $t = 0.1$ ),  $R = 15$  and  $R_\rho = 1.5$ , the stability parameter equals  $R_l = 12$ . Hence, a comparison with the experimental results in table 2 of *Schladow et al.* [1992] confirms that, considering the values of  $R_\rho$  and  $R_l$ , even for this large range of  $R_l$  the simulation undoubtedly falls into Class II. For this regime, self-propagation is therefore possible, and we consider its existence in a slightly larger aspect ratio container.

### 4.3.2 The analysis of self propagation

For the same values of the parameters as in the previous simulation, the evolution of the intrusions is investigated for a wide tank with  $A = 4$ . The numerical resolution in the simulations was chosen to be  $401 * 101$ . This choice was determined by a desire to just resolve the salinity boundary layers but keep the computation manageable in terms of CPU time.

In these simulations, the thermal forcing at the left sidewall is maintained until  $t = 0.05$ . We present the flow development after  $t = 0.05$  for three different cases in the Figs. 4.5. In the Figs. 4.5a, the development of the flow has been plotted for the case that the thermal forcing is

#### 4. The physics behind self-propagating layers

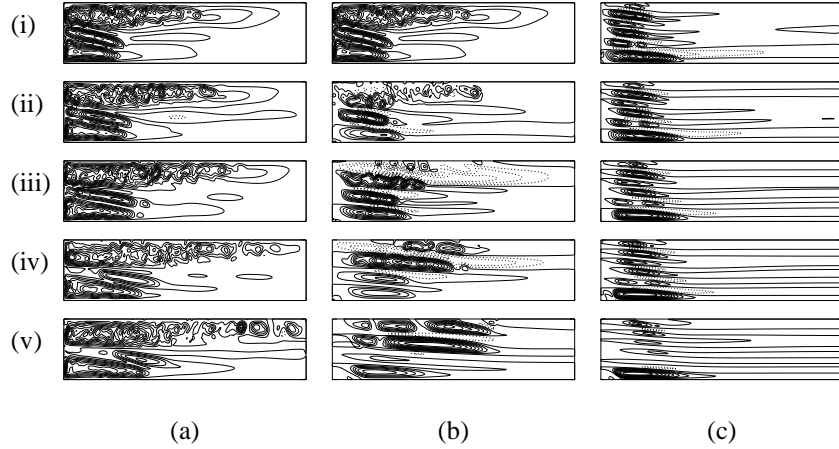


Figure 4.5: *Contour plots of the stream function from  $t = 0.05$  for both doubly stratified and singly stratified cases, for  $A = 4$ . (a): doubly stratified, thermal forcing continued, (b): doubly stratified, no thermal forcing, (c): singly stratified, no thermal forcing. Time intervals: (i) :  $t = 0.05$ , (ii) :  $t = 0.06$ , (iii) :  $t = 0.07$ , (iv) :  $t = 0.09$ , (v) :  $t = 0.1$ .*

continued after  $t = 0.05$ . The layers continue to develop towards the right wall and the region of strong convective activity extends to nearly half the container. If for this case, the thermal forcing is stopped at  $t = 0.05$ , then still the layers continue to propagate towards the right (Fig. 4.5b). The latter is a clear signature of self-propagation and will be analysed below. For comparison, the evolution for the singly stratified case, for which the forcing is turned off at  $t = 0.05$  is also shown (Fig. 4.5c). Self-propagation does not occur and the layers disappear due to viscous dissipation.

The flow in the Figs. 4.5b is considered in more detail by vertical sections of the temperature, salinity and density at different horizontal positions within the layer. At  $t = 0.05$ , it is observed that heat and salt have been transported upwards within the upper layer in Fig. 4.5b, such that the temperature distribution is stabilizing (Fig. 4.6a) and the salinity distribution (Fig. 4.6b) is slightly destabilizing. However, the liquid is still stably stratified (Fig. 4.6c) apart from some small intervals where it is unstably stratified. Hence, the main source of convective activity can be attributed to salt-fingering, with localized areas where direct buoyancy induced convection occurs. As the forcing is turned off, the stabilizing influence of the temperature distribution decreases since thermal diffusion is fast (Fig. 4.6d). The salt transport to the top of the upper layer decreases and consequently maxima in salinity appear within the upper layer (clearest seen

### 4.3. Results

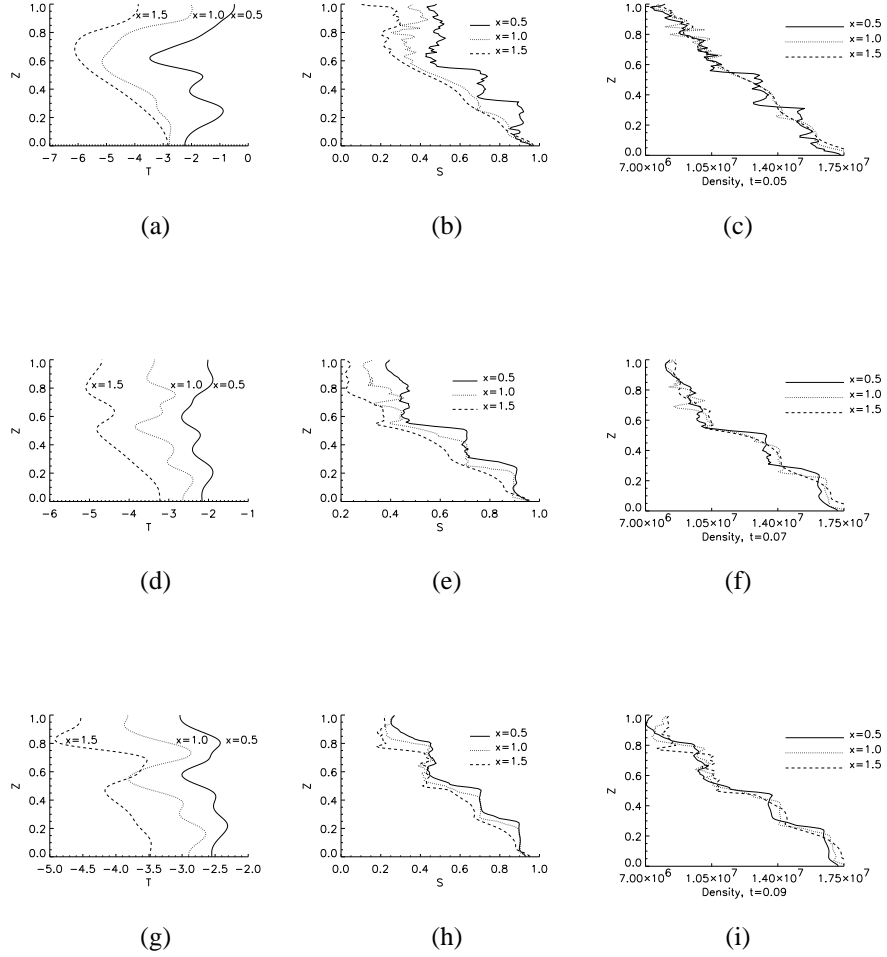


Figure 4.6: Vertical sections of temperature, salinity and density for the doubly stratified ( $A = 4$ ) case at several instants; (a - c):  $t = 0.05$ , (d - f):  $t = 0.07$ , (g - i):  $t = 0.09$ . The horizontal scales for  $T$  and  $S$  differ in order to magnify the differences between the profiles in a plot.

in Fig. 4.6e at  $x = 1.0$ ). The influence on the density is such that the distribution remains stably stratified (Fig. 4.6f). At  $t = 0.09$ , the temperature profiles have reversed near the top of the

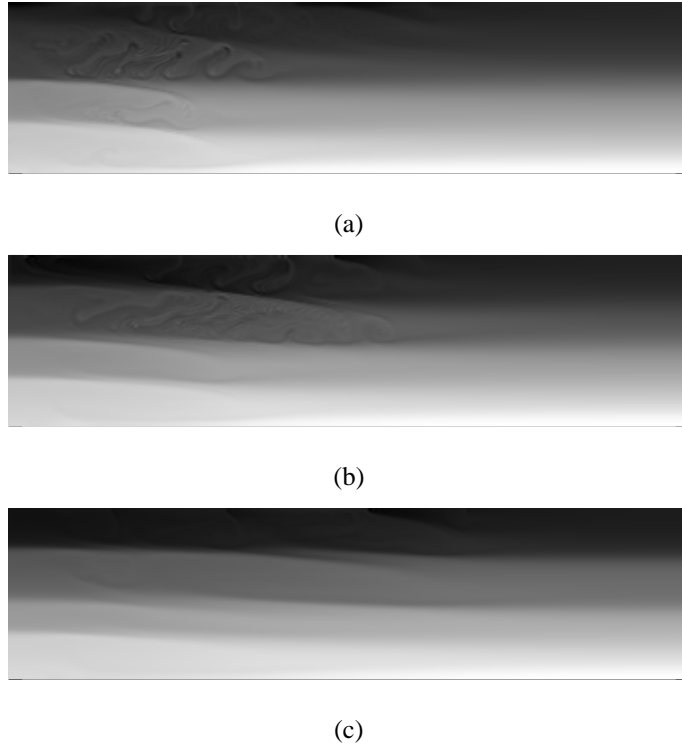


Figure 4.7: *Density grey-shade plots for the doubly stratified case after thermal forcing has been turned off. (a):  $t = 0.07$  (panel (iii) in Fig. 4.5), (b):  $t = 0.09$  (panel (iv) in Fig. 4.5), (c):  $t = 0.15$  (panel (v) in Fig. 4.5).*

upper layer (Fig. 4.6g) and a maximum in the temperature appears near  $z = 0.8$  at  $x = 0.5$  and appears at  $z = 0.7$  at  $x = 1.5$ . A similar shift in the maxima of the salinity profile in the upper layer is observed (Fig. 4.6h) with a larger salinity at  $x = 0.5$  than at  $x = 1.5$ . Consequently, the isopycnals slope towards the horizontal, as can be seen in Fig. 4.6i. This slope is clearly visible in a gray-shade plot of the density at the corresponding times ( $t = 0.07$  and  $t = 0.09$ ) shown in Fig. 4.7a and Fig. 4.7b, respectively. At a later time ( $t = 0.15$ ), this slope decreases due to adjustment (Fig. 4.7c). The corresponding density plots for the singly stratified case (Fig. 4.8a-c) show a much smaller slope and hardly any change with time after the forcing has been turned off.

The horizontal velocity at  $x = 0.5$  (Fig. 4.9a) and  $x = 1.5$  (Fig. 4.9b) for two different times

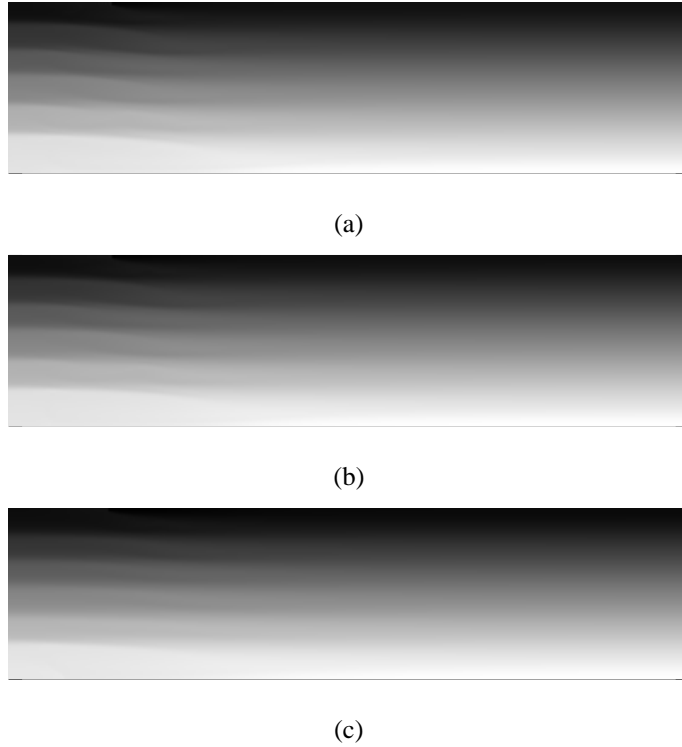


Figure 4.8: As Figure 4.7, but now for the singly stratified case at the same instants.

during the evolution of the flow in Fig. 4.5b are shown in Figs. 4.9. In Fig. 4.9a, the magnitude of the horizontal velocity at about  $z = 0.8$  increases in time, although the forcing is off. The same is seen in Fig. 4.9b, but the maximum occurs at smaller values of  $z$  ( $z = 0.7$ ). The increase in velocity is also observed in the development of the average kinetic energy  $\langle E_k \rangle$  of the flow which is plotted in Fig. 4.10a. In the unforced doubly stratified flow in Fig. 4.5b,  $\langle E_k \rangle$  initially increases up to  $t = 0.08$  and then decreases. For comparison, the evolution of  $\langle E_k \rangle$  is also shown (Fig. 4.10b) for the singly stratified flow in Fig. 4.5c. As is expected,  $\langle E_k \rangle$  decreases immediately as the forcing is turned off due to viscous dissipation.

The flow shown in Fig. 4.5b and its characteristics presented above are a clear example of self-propagation. The main question is how to describe the physics of this phenomenon and identify its energy sources. *Schladow et al.* [1992] suggest that local instabilities induced by liquid blocking due to endwall effects [*Turner, 1973*] are the main energy source of self-propagation.

#### 4. The physics behind self-propagating layers

---

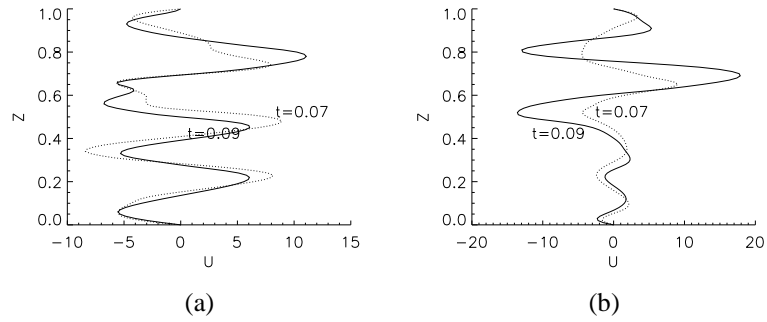


Figure 4.9: Vertical section of the horizontal velocity at  $x = 0.5$  (a) and  $x = 1.5$  (b) for two different times after shut-off of thermal forcing (doubly stratified case).

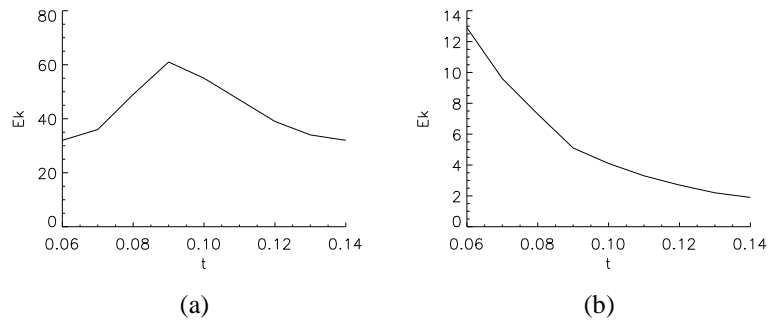


Figure 4.10: Change in  $\langle E_k \rangle$  with time when thermal forcing has been shut off; (a): doubly stratified case (Fig. 4.5b), (b): singly stratified case (Fig. 4.5c).

Characteristic of liquid blocking is a weak upward and downward flow just ahead of the intrusion. This flow disturbs the stabilizing salinity distribution but leaves the unstable temperature distribution merely intact due to the much larger thermal diffusivity. Hence, the value of  $R_\rho$  is

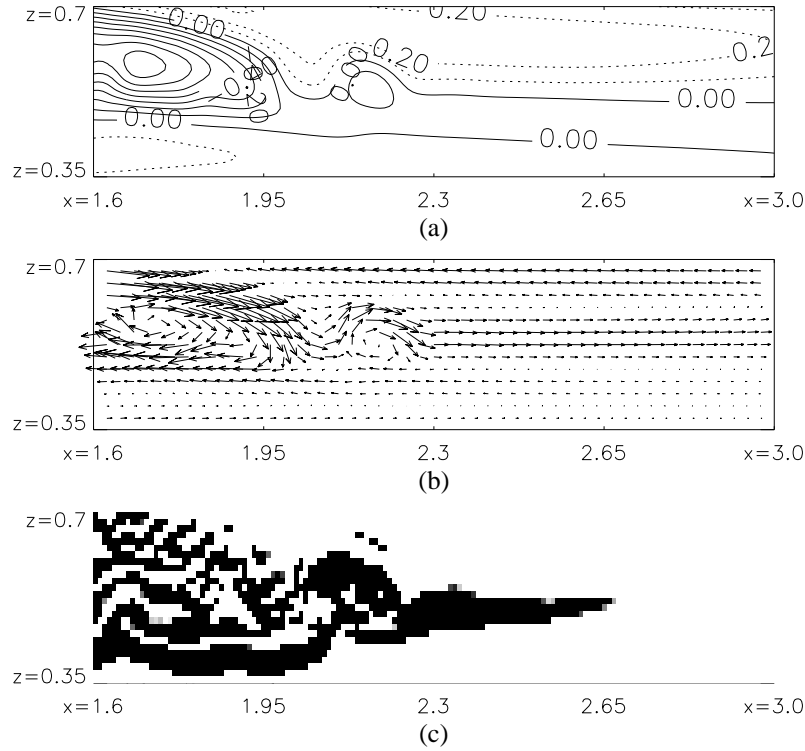


Figure 4.11: Detail of the intrusion front in Figure 4.5b (panel iv) for the doubly stratified case; (a):  $\psi$  near intrusion front, (b) velocities (for clarity a reduced number of vectors is shown), (c)  $R_\rho$ , black regions correspond to  $R_\rho < 1$ .

locally reduced and local instabilities provide the energy for the intrusion to grow.

To test this hypothesis, the flow just ahead of the intrusions is considered during the self-propagation stage. The streamfunction field (Fig. 4.11a), a vector plot of the velocity (Fig. 4.11b) and the  $R_\rho$  field (Fig. 4.11c) are plotted just ahead of the propagating intrusion (detail of figure 4.5b(iv)). Note the different vertical scale in this plot, compared to the ones in Fig. 4.5b. Although there is a weak buoyancy driven flow ahead of the intrusions, there are no signatures of a blocked flow ahead of the intrusion (Fig. 4.11a-b). The background flow is nearly parallel and returns only in a thin boundary layer near the right wall. The black regions in Fig. 4.11b indicate values of  $R_\rho < 1$  and show that the flow ahead of the intrusion is statically unstable. This is caused by an unstable thermal stratification and a strongly reduced salinity gradient.

#### 4. The physics behind self-propagating layers

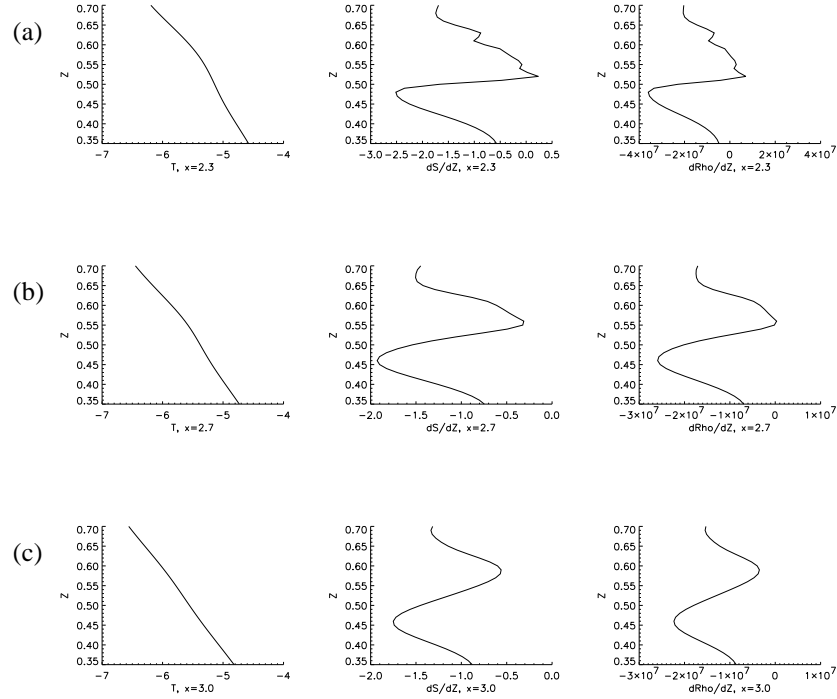


Figure 4.12: Vertical sections of temperature, vertical salinity gradient and vertical density gradient ahead of the intrusion front; (a)  $x = 2.3$ , (b)  $x = 2.65$ , (c)  $x = 3.0$ .

The Figs. 4.12a-c show that the temperature field farther ahead of an intrusion is indeed undisturbed, but that the salinity field is affected by the weak background flow. The vertical scale over which the unstable stratification occurs is sufficiently large (about 0.1 units) to cause a buoyancy driven direct instability. Even if the stratification is stable, double-diffusive instabilities may cause growth of perturbations ahead of the intrusions.

However, the origin of the weak background flow is the gravitational adjustment associated with the sloping isopycnals and is not related to any blocking. This can be seen in the Figs. 4.5b (panels (iii) and (iv)), where the flow in the upper layer is to the right along the first interface, just as one would expect from an adjustment. Moreover, one can observe the adjustment in the Figs. 4.7a-c. Hence, local instabilities may provide an energy source of the self-propagation of the intrusions, but only in the presence of such a weak background flow, induced by adjustment.

## 4.4 Conclusions

The results from the two-dimensional numerical simulations of the evolution of intrusions into a stratified liquid show many features also observed in experiments. This *a posteriori* justifies the use of the two-dimensional model; the dominant physics of layer formation and self-propagation is already captured by such a model.

The analysis of the flow details lead to the following physical picture of self-propagation in doubly stratified systems. If the vertical stability ratio  $R_\rho$  is small enough, the upward transport of salt along the heated wall is able to cause intense convection in the upper layer through salt-fingering (or direct instabilities). This cannot be accomplished in a singly stratified liquid, because (i) the initial temperature distribution does not destabilize the flow and (ii) the layer thickness does not increase but decreases upwards. Hence, most of the salt is transported by the lowest layers in this case, contrary to that in the doubly stratified case, where most salt is transported by the most upper layer.

As the lateral temperature forcing is turned off, a horizontal salt gradient results because near the heated wall more salt has accumulated than far from that wall. Contrary to the temperature distribution, the salinity distribution recovers slowly. Consequently, a relatively strong slope in the isopycnals results when the sidewall heating is turned off. During the unforced evolution, the liquid adjusts itself and the heavier liquid moves to its neutral level. This sets up a background flow and provides a simple source of energy of self-propagation. Due to the presence of the background flow the salinity field is modified just ahead of the intrusion whereas the temperature field is hardly modified because of relatively large thermal diffusion. Local instabilities, which may be direct or diffusively driven, may provide kinetic energy to the intrusion.

Hence, the heart of the physics of the self-propagation is the slope of the isopycnals set-up by the differential salt transport in the upper layer due to salt fingering. This slope provides itself an energy source due to adjustment and provides the background flow such that local instabilities may occur. When the stability ratio increases, both sources of energy are much weaker since the slope in the isopycnals is much smaller and no background flow (and consequently no local instabilities) occurs. This description therefore explains why self-propagation does not occur in singly stratified systems.

# References

- Jacobs, S. S., Huppert, H. E., Holdsworth, G., Drewry, D. J., Thermohaline steps induced by melting of the Erebus Glacier tongue, *J. Geophys. Res.*, **86**, 6547–6555 (1981).
- Jeevaraj, C., Imberger, J., Experimental study of double-diffusive instability in sidewall heating, *J. Fluid Mech.*, **222**, 565–586 (1991).
- Kranenborg, E.J, Dijkstra, H.A., The evolution of double-diffusive intrusions into a stably stratified liquid. I: A study of the layer merging process. *Int. J. Heat Mass Transfer*, submitted, (1996).
- Schladow, S. G., Thomas, E., Koseff, J. R., The dynamics of intrusions into a thermohaline stratification, *J. Fluid Mech.*, **236**, 127–165 (1992).
- Schmitt, R.W., Double diffusion in oceanography, *Ann. Rev. Fluid Mech.*, **26**, 255-285 (1994).
- Turner, J. S., *Buoyancy effects in fluids*, Cambridge (1973).
- Wirtz, R. A., Briggs, D. G., Chen, C. F., Physical and numerical experiments on layered convection in a density-stratified fluid, *Geophysical Fluid Dynamics* , **3**, 265–288 (1972).